Bound states in the three-dimensional electron gas with repulsive or attractive test charges: many-body effects

1996 J. Phys.: Condens. Matter 8 7393

(http://iopscience.iop.org/0953-8984/8/40/006)

J. Phys.: Condens. Matter **8** (1996) 7393–7409. Printed in the UK

Bound states in the three-dimensional electron gas with repulsive or attractive test charges: many-body effects

A Gold† and A Ghazali‡

† Laboratoire de Physique des Solides, Université Paul-Sabatier, 118 Route de Narbonne, 31062 Toulouse, France

‡ Groupe de Physique des Solides, Universités Paris 7&6, 2 place Jussieu, 75251 Paris, France

Received 22 May 1996

Abstract. In the low-density regime *bound states* between *negative* (repulsive) test charges are obtained when many-body effects (exchange and correlation) are incorporated in the screening function of the three-dimensional electron gas via the local-field correction. The Schrödinger equation is solved in the momentum space by diagonalizing the corresponding matrix. We also perform variational calculations and find good agreement between the two methods. For high electron density $r_s < r_{sc} \approx 6$–8 (r_s is the density parameter) no bound states are found. Below a critical density $r_s > r_{sc}$ the number and the energy of bound states increase with decreasing electron density. For large r_s the binding energy for the ground state saturates near -0.065 Ryd*. We discuss the wave functions of the ground state and of the lowest excited states. We also present results for the effects of exchange and correlation for a positive (attractive) test charge and we discuss results for the ground state and excited states.

1. Introduction

It is well known that a test charge in a three-dimensional electron gas is screened at large distances [1, 2]. In addition, the screened potential exhibits Friedel oscillations [3]. One could ask whether a bound state can occur in the attractive part of these Friedel oscillations. Friedel oscillations occur already within the framework of the random-phase approximation (RPA). Recently, it was argued that many-body effects, described by the local-field correction (LFC), strongly modify the screening properties of a two-dimensional electron gas at low density and enhance Friedel oscillations [4]. In fact it was shown that for a negative test charge many-body effects give rise to bound states in the low-density range of the quasi-one-dimensional [5] and the two-dimensional [6] electron gases. In this paper we study the three-dimensional electron gas and we show that bound states exist, too. However, the binding energy is small compared to the effective Rydberg. In order to describe many-body effects we use the concept of the LFC for the dielectric screening function in the formulation of Singwi and coworkers [7]. (For a review, see [8]). A sum-rule approach to this theory was published recently where the LFC was given in analytical form [9].

For a positive test charge screened by a three-dimensional electron gas a bound state can exist only for a density lower than a critical one, which is Mott's (M) critical density N_M [10]. The possibility of bound states for equally charged particles was suggested in the literature in the early sixties and studied for a short-range potential [11]. In the low-density region a Wigner crystal is expected [12]. Paired electron crystals have been predicted

0953-8984/96/407393+17$19.50

recently in the low-electron-density regime [13]. In fact, we show that in the low-density regime the screened potential of a negative test charge becomes strong enough to produce a bound state with another negative test charge.

We believe that our results for a repulsive screened test charge are novel and these results are discussed in detail in the present paper. The screened attractive test charge has been discussed before in the literature and, therefore, we describe very briefly some new results, mainly concerning excited states.

The paper is organized as follows. In section 2 we describe the model and the theory. Our results for repulsive test charges concerning the exact method to solve the Schrödinger equation and the variational approach are described in section 3. Some results for a screened positively charged impurity are presented in section 4. We comment on our results in section 5 and conclude in section 6.

2. Model and theory

2.1. The screened Coulomb interaction

As the model we use a three-dimensional electron gas with a parabolic dispersion. Distances are expressed in units of the effective Bohr radius $a^* = \varepsilon_L/m^*e^2$ with the Planck constant $h = 2\pi$. Wave numbers are expressed in units of the inverse Bohr radius. m^* is the effective mass and ε_L is the dielectric constant of the background. Energy values are expressed in units of the effective Rydberg $\mathrm{Ryd}^* = m^*e^4/2\varepsilon_L^2$. The density parameter r_s is given by $r_s = [3/4\pi Na^{*3}]^{1/3}$ and $r_s a^*$ is the Wigner–Seitz radius. $N = k_F^3/3\pi^2$ is the three-dimensional electron density and k_F is the Fermi wave number with $k_F a^* = 1.92/r_s$. The Fermi energy ε_F is given as $\varepsilon_F/\mathrm{Ryd}^* = (9\pi/4)^{2/3}/r_s^2 = 3.683/r_s^2$. We consider a test charge screened by the electron gas of density N. The motivation for using a test charge is that the screened potential is known if the LFC for charge density fluctuations is known.

The Coulomb interaction potential in the Fourier space between a (fixed) negative test charge and another negative test charge is repulsive and given by $V_t(q) = 4\pi e^2/\varepsilon_L q^2$. If the interaction is screened by an electron gas the screened interaction potential $V_{sc,t}(q)$ is written as $V_{sc,t}(q) = V_t(q)/\varepsilon(q)$. In section 4 we study an attractive test charge with $V_t(q) = -4\pi e^2/\varepsilon_L q^2$. The dielectric function $\varepsilon(q)$, calculated within the RPA and including the LFC $G(q)$, is given by [1, 2]

$$\frac{1}{\varepsilon(q)} = 1 - \frac{V(q)X_0(q)}{1 + V(q)[1 - G(q)]X_0(q)}. \tag{1}$$

$X_0(q)$ is the Lindhard function in three dimensions [1] and $V(q)$ is the bare interaction potential $V(q) = 4\pi e^2/\varepsilon_L q^2$. For $G(q) = 0$ one obtains the RPA expression $\varepsilon(q) = 1 + V(q)X_0(q)$ [1]. In our calculation we use for $G(q)$ the sum-rule approximation [9] of the Singwi–Tosi–Land–Sjölander (STLS) approach [7]. Analytical results have been obtained within a generalized Hubbard form for the LFC as [9]

$$G(q) = r_s^{3/4}\frac{0.846q^2}{2.188q_0^2C_{13}(r_s) + q^2C_{23}(r_s)} \tag{2}$$

where $q_0 = 12^{1/4}/r_s^{3/4}a^*$ is a characteristic wave number. In the Hubbard approximation (HA) [14] only exchange effects are included. Within the HA for the LFC the coefficients for the LFC are given by $C_{13HA} = 1.096r_s^{1/4}$ and $C_{23HA} = 1.69r_s^{3/4}$ [9]. Equation (2) contains exchange and correlation effects via the coefficients $C_{13}(r_s)$ and $C_{23}(r_s)$ (two-sum-rule approach). The STLS approach does not satisfy the compressibility sum rule [1]. This

is a well known defect of this theory [7]. In equation (19) we describe an LFC $G_c(q)$ which satisfies the compressibility sum rule and gives results quantitatively similar to those of the calculation with $G(q)$.

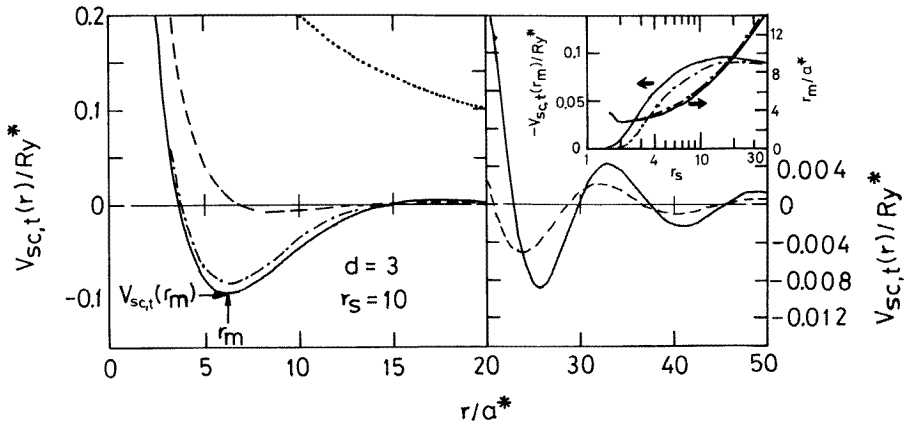

Figure 1. Screened Coulomb potential $V_{sc,t}(r)$ of a repulsive test charge against distance r for $r_s = 10$ as the solid line. The dotted line represents the unscreened potential. The dashed line represents the RPA approximation. In the inset we show $V_{sc,t}(r_m)$ and r_m versus r_s. The dashed–dotted lines represent results calculated by using $G_c(q)$ as given in equation (19).

In the real space the screened Coulomb interaction is given by

$$V_{sc,t}(r) = \frac{1}{2\pi^2 r}\int_0^\infty \mathrm{d}q\, q\sin(qr)V_{sc,t}(q). \tag{3}$$

A representative example for $V_{sc,t}(r)$ is shown in figure 1 for r_s=10 with a minimum $V_{sc,t}(r_m) = -0.093$ Ryd* at $r_m = 6.3a^*$. Note that the attractive part is strongly enhanced by the LFC as compared to the RPA one. The corresponding values for $r_s = 20$ are $V_{sc,t}(r_m) = -0.097$ Ryd* and $r_m = 9.3a^*$. A systematic study of r_m and $V_{sc,t}(r_m)$ versus r_s (see the inset in figure 1) shows that $V_{sc,t}(r_m)$ presents a weak maximum and saturates at large r_s at about -0.09 Ryd*. $V_{sc,t}(r_m)$ becomes very small for $r_s < 2$. We note that r_m is quite large in the low-density range, which means that bound states, if any, are very extended.

Friedel oscillations of the screened potential are shown in the right-hand side of figure 1. Many-body effects increase the amplitude of Friedel oscillations; however, the effect is relatively small: the enhancement is about a factor two for $r_s = 10$. On the other hand we conclude from figure 1 that the attractive minimum within the RPA at $r_m = 8.5a^*$ with $V_{sc,t}(r_m) = -0.008$ Ryd* is enhanced by many-body effects by a factor of 12: $V_{sc,t}(r_m) = -0.0923$ Ryd*. We shall show that for $r_s = 10$ the binding energy for the ground state is -0.0207 Ryd*.

In order to show that bound states exist in the screened potential one has to solve the Schrödinger equation for a test charge moving in the external potential. $V_{sc,t}(r)$ is a central potential and only depends on r. Accordingly, the angular dependence of the wave function in the real space and in the momentum space is described by spherical harmonics $Y_{lm}(\varphi, \theta)$. It is immediately clear that states with given angular momentum l are degenerate with respect to the quantum number m and the degeneracy is $g_l = (2l + 1)$. However, states with different values of l are not degenerate, as in the bare attractive hydrogen atom. For

the screened potential this accidental degeneracy [15] found in the hydrogen atom is lifted.

One can use for the wave function $\psi(\boldsymbol{r}) = \phi_{n_r l}(r)Y_{lm}(\varphi, \theta)$ and one finds for $\phi_{n_r l}(r)$ the radial Schrödinger equation for the effective potential $V_{eff}(r) = V_l(r) + V_{sc,t}(r)$ with $V_l(r) = l(l+1)/2m^*r^2$. $V_{eff}(r)$ is strongly repulsive at small distances, $V_{eff}(r \to 0)/\mathrm{Ryd}^* = l(l+1)a^{*2}/r^2 + 2a^*/r$. From general arguments [15] it is clear that for $l > 0$ the behaviour of the wave function for small r is determined by $V_l(r)$. As for the hydrogen atom we conclude that for $l > 0$ $\phi_{n_r l}(r \to 0) \propto r^l$. In the momentum space $\psi(\boldsymbol{q}) = \phi_{n_r l}(q)Y_{lm}(\theta, \varphi)$ and $\phi_{n_r l}(q \to 0) \propto q^l$ [16]. In the following we will use as notation ϕ or ϕ_l for $\phi_{n_r l}$.

2.2. The Schrödinger equation in momentum space

The Schrödinger equation for the screened potential can only be solved numerically and we choose to solve the Schrödinger equation in the momentum space. The reason for this is that the screened potential is readily given in momentum space (see equation (1)). As we will show below, the present method is accurate and fast enough and might be used for potentials which do not have spherical symmetry. The Schrödinger equation in the momentum space is given by

$$\frac{q^2}{2m}\psi(\boldsymbol{q}) + \frac{1}{8\pi^3}\int \mathrm{d}^3\boldsymbol{q}'\, V_{sc,t}(\boldsymbol{q}-\boldsymbol{q}')\psi(\boldsymbol{q}') = E\psi(\boldsymbol{q}). \tag{4}$$

Using spherical coordinates, we have discretized the integral over $\boldsymbol{q}'$ in equation (4) according to a set of (q', θ',φ'). The sampled values in q', θ', and φ' are those used in Gauss routines for integration. Two, three, or four adjacent intervals in q', θ', and φ' are used in order to correctly sample the integral. In this way the Hamiltonian operator in equation (4) is discretized under the form of a matrix. The order of this matrix is 3200 (2×8 points for $0 \leqslant q'a^* < 2$, 2×5 points for $0 \leqslant \theta' \leqslant \pi$ and 4×5 points for $0 \leqslant \varphi' \leqslant 2\pi$). The eigenenergy and eigenfunction problem are then solved numerically by a standard method for matrix diagonalization.

We have checked the accuracy of our method by comparing the eigenfunctions and eigenenergies thus obtained with those of known problems, such as the three-dimensional attractive Coulomb problem. Not only eigenenergies but also eigenfunctions are calculated with a good accuracy. Note, however, that any discretization introduces a systematic lifting of the degeneracy because it acts as a perturbation to the true Hamiltonian, which is defined in the continuous momentum space. The lifting of the degeneracy, however, is small. In addition, as in other numerical solutions, the bound states are less accurately determined when they are more excited.

3. The screened repulsive test charge

3.1. Matrix diagonalization

We first discuss the energy values for bound states versus r_s. For $r_s < 6$ no bound states have been found. For $6 \leqslant r_s < 11$ we find one bound state ($l = 0$, $g_l = 1$). Its energy is given in the inset of figure 2. The binding energy approaches zero for $r_s = r_{sc} = 6$ and r_{sc} is the critical density parameter. Our variational results are also shown in the inset and give a smaller binding energy; where the binding energy vanishes $r_{sc} = 7$. It is known that the variational method gives too small binding energies, especially when the binding energy becomes small. For $r_s \geqslant 11$ we find excited bound states. Our results for the bound states

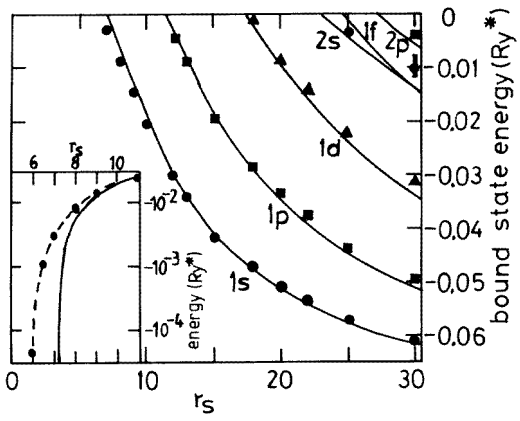

Figure 2. Bound state energies E_{num} for a screened repulsive test charge found by matrix diagonalization against r_s as dots ($l = 0$), squares ($l = 1$), triangles ($l = 2$), and bars ($l = 3$). The variational results E_{min} (characterized by $n_r l$) are shown as solid lines. In the inset we show the ground state energy versus r_s for $5 < r_s < 11$ with a logarithmic energy scale.

obtained with the method of matrix diagonalization versus r_s ($0 < r_s < 30$) are shown in figure 2 as solid symbols. The solid lines represent the variational calculation, as discussed in subsection 3.2. Figure 2 contains the complete information about the ground state and the excited states. We denote the states by two quantum numbers, the radial quantum number n_r and the angular quantum number l.

With our numerical method we also obtain all information about the eigenfunctions. The eigenfunctions, which we obtain numerically, are the eigenfunctions $\psi(q, \theta, \varphi)$ in the momentum space. In order to characterize the angular momentum l of the bound states three methods have been applied: (i) the (quasi-) degeneracy of the eigenenergy, (ii) the behaviour of the wave function at small wave numbers, and (iii) the angular dependence of the wave function. However, details are not given in this paper.

The eigenfunctions can be Fourier transformed to obtain the eigenvectors in the normal space. This method has been applied; however, the numerical inaccuracy in the $\boldsymbol{q}$-space is reinforced in the $\boldsymbol{r}$-space. Therefore, we do not give here the results obtained with this method. Instead, using the (θ, φ) symmetry of the angular part of the wave function one can show that [16]

$$\phi_l(r) \propto \frac{1}{r} \int_0^\infty \mathrm{d}q' q' j_l(q'r) \phi_l(q') \tag{5}$$

and $j_l(x)$ is the spherical Bessel function of the first kind of order l. For the ground state wave function one has to use $j_0(x) = \sin(x)$. It follows immediately that $\phi_0(r \to 0) =$ constant. In fact, in order to obtain the radial dependence of $\psi(r, \theta, \varphi)$ one can use in equation (5) $\psi(q, \theta', \varphi')$ instead of $\phi_l(q')$. Numerical results for the ground state $\psi(r, \theta, \varphi)$ versus r are shown in figure 3 for $r_s = 20$. For $r = 0$ we find a very small finite value and we cannot decide whether this is a true effect or a numerical error. However, $\psi(r, \theta, \varphi) = \phi(r) Y_{00}(\theta, \varphi)$ shows a large peak at about $r^* = 10a^*$, which corresponds to the value r_m, where the screened potential shows a strong minimum.

The ground-state wave function in the q-space is shown in figure 4. Note that near $qa^* = 0.4$ the wave function $\psi(q, \theta, \varphi) = \phi_0(q) Y_{00}(\theta, \varphi)$ changes its sign and it decays very rapidly for $qa^* > 1$. The numerical results are in very good agreement with our results

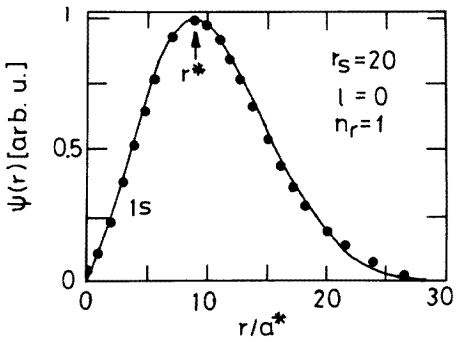

Figure 3. Wave function $\Psi(r)$ of the ground state ($n_r = 1, l = 0$) for a screened repulsive test charge for r_s=20 against r. The solid dots are the numerical results of the matrix diagonalization and the solid line represents the variational calculation with $\alpha = 7.54a^*$ and $k_1 = 2.80$.

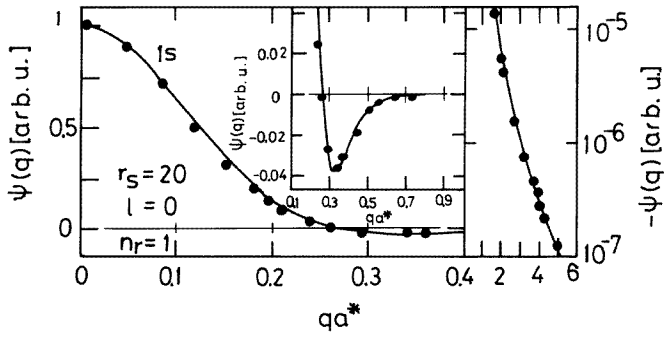

Figure 4. Wave function $\Psi(q)$ of the ground state ($n_r = 1, l = 0$) for a screened repulsive test charge for r_s=20 against q. The solid dots are the numerical results of the matrix diagonalization and the solid line represents the variational calculation with $\alpha = 7.54a^*$ and $k_1 = 2.80$.

obtained with a variational wave function (see the solid line in figure 4) as described in the next section.

3.2. The variational wave function

Using a trial wave function $\phi_v(r)$ the variational energy E_{var} is given by

$$E_{var} = \langle T \rangle + \langle V_l \rangle + \langle V_{sc,t} \rangle \tag{6}$$

where $\langle O \rangle = \int_0^\infty \mathrm{d}r r^2 \phi_v(r) O \phi_v(r)$. For certain simple wave functions the r-integrals for $O = T$, V_l and $V_{sc,t}$ can be calculated analytically.

The screened potential near the minimum at r^* can be described by a one-dimensional oscillator potential. Therefore we use as a variational wave function

$$\phi_{1v}(r) = A r^{k_1/2} \mathrm{e}^{-r^2/2\alpha^2} \tag{7}$$

with the normalization constant A given by $A^2 = 2/\Gamma[(k_1 + 3)/2]\alpha^{3+k_1}$. k_1 and α are the variational parameters. It should be noted that $\phi_{1v}(r)$ describes states with a certain angular momentum l: the radial Schrödinger equation contains the part $V_l(r)$ and $\Psi(\boldsymbol{r}) = \phi_{1v}(r) Y_{lm}(\theta, \varphi)$. $\phi_{1v}(r)$ has one node $n_r = 1$ at $r = 0$ if $k_1 > 0$. Solving

the variational problem with this wave function gives bound states with quantum numbers $n_r = 1$ and $l = 0, 1, 2, 3, \ldots$. Radial wave functions with two nodes have a small binding energy and are discussed later.

We obtain for the radial wave function with $n_r = 1$ and characterized by k_1 and α the following analytical results:

$$\langle T \rangle = \mathrm{Ryd}^*(a^{*2}/\alpha^2)(2k_1 + 3)/(2k_1 + 2) \tag{8}$$

$$\langle V_l \rangle = \mathrm{Ryd}^*(a^{*2}/\alpha^2)2l(l + 1)/(k_1 + 1) \tag{9}$$

and

$$\langle V_{sc,t} \rangle = \frac{4}{\pi}\mathrm{Ryd}^* a^* \int_0^\infty \mathrm{d}q \, \frac{{}_1F_1[(3 + k_1)/2; 3/2; -q^2\alpha^2/4]}{\varepsilon(q)}. \tag{10}$$

${}_1F_1(x; y; z)$ is the degenerate hypergeometric function [17]. Note that $\varepsilon(q)$ together with the LFC depends on r_s. Consequently, the variational parameters k_1 and α, at $E = E_{min}$, depend on r_s and on the form chosen for the LFC. This variational approach can be easily applied when other expressions for the LFC become available in the literature. Our result obtained for $l = 0, 1, 2 \ldots$ are given in figure 5. Note that the states are very extended in the normal space as is shown by the large values found for α. In fact, figure 5 is the only figure where the reader can find information about the extension of the wave function as function of r_s: the wave function $\phi_{1v}(r)$ shows a maximum at r^* given by $r^* = (k_1/2)^{1/2}\alpha$.

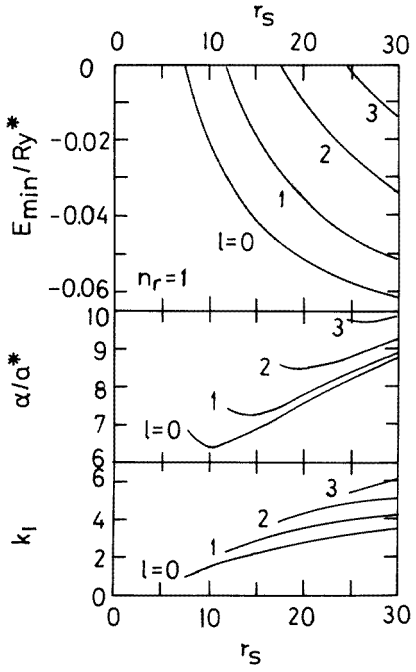

Figure 5. Minimal energy E_{min} with $\psi_{1v}(r)$ and variational parameters α and k_1 for a screened repulsive test charge against r_s for $n_r = 1$ and $l = 0, 1, 2, 3$.

For the states with two nodes $n_r = 2$ we use for the radial wave function

$$\phi_{2v}(r) = B(r^{k_2/2} - Cr^{k_3/2})\,\mathrm{e}^{-r^2/2\beta^2}. \tag{11}$$

This radial wave function describes the states with $n_r = 2$ and $l = 0, 1, 2, \ldots$. The following analytical results for the variational energy are derived:

$$\langle T\rangle = \mathrm{Ryd}^*\frac{a^{*2}}{8}B^2\beta^{k_2+1}\{\Gamma([k_2+1]/2)(2k_2+3) + C^2\beta^{k_3-k_2}\Gamma([k_3+1]/2)(2k_3+3) + C\beta^{k_3/2-k_2/2}\Gamma([k_2/2+k_3/2+1]/2)(k_2^2/2+k_3^2/2-k_2k_3-2k_2-2k_3-6)\} \tag{12}$$

$$\langle V_l\rangle = \mathrm{Ryd}^*\frac{a^{*2}}{2}l(l+1)B^2\beta^{k_2+1}\{\Gamma([k_2+1]/2) + C^2\beta^{k_3-k_2}\Gamma([k_3+1]/2) - 2C\beta^{k_3/2-k_2/2}\Gamma([k_2/2+k_3/2+1]/2)\} \tag{13}$$

$$\langle V_{sc,t}\rangle = \frac{2}{\pi}\mathrm{Ryd}^*a^*B^2\int_0^\infty \mathrm{d}q\,\frac{1}{\varepsilon(q)}\{\beta^{k_2+3}\Gamma([k_2+3]/2)_1F_1[(3+k_2)/2;\,3/2;\,-q^2\beta^2/4] - 2C\beta^{k_2/2+k_3/2+3}\Gamma([k_2/2+k_3/2+3]/2)_1F_1[(6+k_2+k_3)/4;\,3/2;\,-q^2\beta^2/4] + C^2\beta^{k_3+3}\Gamma([k_3/2+3]/2)_1F_1[(3+k_3)/2;\,3/2;\,-q^2\beta^2/4]\}. \tag{14}$$

With the normalization condition $\langle\phi_{2v}|\phi_{2v}\rangle = 1$ we find

$$1/B^2 = \{\beta^{k_2+3}\Gamma([k_2+3]/2) - 2C\beta^{k_2/2+k_3/2+3}\Gamma([k_2/2+k_3/2+3]/2) + C^2\beta^{k_3+3}\Gamma([k_3+3]/2)\}/2. \tag{15}$$

The condition for C follows from the fact that $\langle\phi_{1v}|\phi_{2v}\rangle = 0$ and we obtain

$$C = \left[\frac{2\alpha^2\beta^2}{\alpha^2+\beta^2}\right]^{k_2/4-k_3/4}\frac{\Gamma([k_1/2+k_2/2+3]/2)}{\Gamma([k_1/2+k_3/2+3]/2)}. \tag{16}$$

Our results E_{min} of the variational approach for $n_r = 1$ and $n_r = 2$ are shown in figure 2.

Using the spherical Bessel functions $j_l(x)$ the wave functions $\phi_l(r)$ can be Fourier transformed. One obtains [17]

$$\phi_l(q) \propto \frac{1}{q}\int_0^\infty \mathrm{d}r\,r\,j_l(qr)\phi_l(r). \tag{17}$$

For $l = 0$ the wave function in the momentum space is given by $\phi_l(q \to 0) =$constant. For $n_r = 1$ and $n_r = 2$ the variational wave functions in the momentum space can be expressed in terms of degenerate hypergeometric functions [17]. We only give the explicit results for $n_r = 1$ and $l = 0$ because equation (17) can be used directly to calculate $\phi_l(q)$. The Fourier transforms of the variational wave functions can be compared directly with the results of the matrix diagonalization. For the ground-state wave function with $n_r = 1$ and $l = 0$ we find the explicit result [17]

$$\phi_{1v}(q) \propto {}_1F_1[(6+k_1)/4;\,3/2;\,-q^2\alpha^2/2). \tag{18}$$

Our results for the variational ground-state wave function for $r_s = 20$ are shown in figure 4 and agree very well with the numerical results. We mention that the large q-dependence is in very good agreement with the numerical results.

For the first (1p) excited state the variational results for the wave function in the momentum space are shown in figure 6 and are in reasonable agreement with the corresponding results of the matrix diagonalization. The variational result for the r-dependence (inset) and the q-dependence of the 2s state wave function with $n_r = 2$ and $l = 0$ are shown in figure 7 together with numerical results.

We have also applied the variational method with the variational wave function $\phi_{3v}(r) = Ar^{k_4/2}\exp(-r/2\delta)$ where $k_4 = 1, 2, 3, 4$ and δ is the variational parameter. These wave functions describe the states $n_r = 1$ and $l = 0, 1, 2, \ldots$. This wave function represents for $k_4 = 0$ and $\delta = a^*$ the ground-state wave function of the hydrogen atom with an

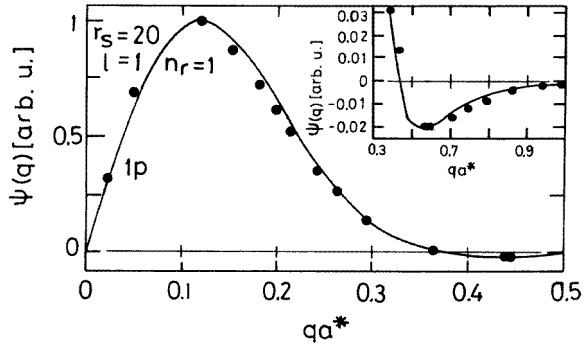

Figure 6. Wave function $\psi(q)$ of the first excited state ($n_r = 1, l = 1$) for a screened repulsive test charge for $r_s = 20$ against q. The solid dots are the numerical results of the matrix diagonalization and the solid line represents the variational calculation with $\alpha = 7.80a^*$ and $k_1 = 3.45$.

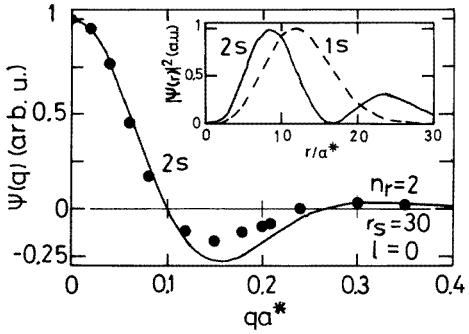

Figure 7. Wave function $\psi(q)$ of the excited state ($n_r = 2, l = 0$) for a screened repulsive test charge for $r_s = 30$ against q. The solid dots are the numerical results of the matrix diagonalization and the solid line represents the variational calculation with $\beta = 10.25a^*$, $k_2 = 4.482$ and $k_3 = 4.480$. In the inset we show $|\psi(r)|^2$ for the 2s state (solid line) and the 1s state (dashed line).

unscreened attractive Coulomb potential. The binding energy obtained with $\phi_{3v}(r)$ is in good agreement (8%) with results obtained by using $\phi_{1v}(r)$ (figure 2). Nevertheless, the energy values found with the Gaussian variational form $\phi_{1v}(r)$ are somewhat lower than for the exponential form.

3.3. Different approximations for the LFC

We mention that one does obtain bound states within the HA. Some values for the binding energy of the ground state for large r_s calculated with $\phi_{1v}(r)$ are given in table 1. Note that the binding energies are much smaller than if calculated with the full LFC, where exchange and correlation effects are included. In table 1 we present some results for very large r_s. Note that for $r_s = 100$ the Fermi energy is very small, $\varepsilon_F = 3.7 \times 10^{-4}$ Ryd*, and disorder effects are certainly relevant in real systems. Within the HA a systematic study versus r_s showed that bound states only exist for $r_s > r_{scHA} = 12.6$.

Table 1. Ground state energies E_{min} and variational parameters α and k_1 for a screened repulsive test charge found by the variational method with $\phi_{1v}(r)$ using the LFC, the Hubbard approximation (HA), and the RPA for different density parameters. The value r_{sc}, where the ground-state energy vanishes, is also given.

r_s	E_{min}/Ryd*($\alpha/a^*\|k_1$) LFC ($r_{sc} = 7.2$)	E_{min}/Ryd* ($\alpha/a^*\|k_1$) HA ($r_{sc,HA} = 12.6$)	E_{min}/Ryd* ($\alpha/a^*\|k_1$) RPA ($r_{sc,RPA} = 57.5$)
100	−0.0607 (15.0|6.6)	−0.0109 (21.7|6.3)	−0.000 489 (34.9|4.8)
80	−0.0629 (13.6|5.9)	−0.0116 (19.4|5.7)	−0.000 361 (31.7|4.2)
60	−0.0658 (11.8|5.2)	−0.0124 (16.8|4.9)	−0.000 067 (28.8|3.4)
40	−0.0657 (8.9|4.1)	−0.0127 (13.9|3.9)	—
30	−0.0617 (8.8|3.6)	−0.0120 (12.2|3.3)	—
20	−0.0515 (7.5|2.8)	−0.0089 (10.6|2.4)	—
15	−0.0416 (6.8|2.3)	−0.0039 (10.0|1.8)	—
10	−0.0195 (6.4|1.6)	—	—

Even within the RPA we find a bound state at very low density, however, the binding energy is extremely small. Some results are given in table 1. Using $\phi_{1v}(r)$ we have studied in detail the behaviour of the binding energy of the ground state against r_s and found that bound states only exists for $r_s > r_{scRPA} = 57.5$. Including the LFC we found bound states for $r_s > r_{sc} = 6$. We conclude that $r_{scRPA}/r_{sc} = 9.58$ which means that $N_c/N_{cRPA} = 880$.

The calculations reported in this subsection show that the existence of a bound state in a screened repulsive potential is not a special property of the LFC. In fact, for $G(q) = 0$ the bound state is induced by Friedel oscillations. However, for $r_s = 100$ the bound-state energy value is increased by a factor of 148 if many-body effects via the LFC are included.

In order to show that the chosen form of the LFC is not an *ad hoc* trick to produce a bound state for a screened repulsive test charge a more elaborate three-sum-rule approach for the LFC was formulated [18]. There the LFC is given by

$$G_c(q) = r_s^{3/4} \frac{0.846q^2}{2.188q_0^2 C_{13c}(r_s) + q^2 C_{23c}(r_s) - q_0 q C_{33c}(r_s)}. \tag{19}$$

The coefficient $C_{13c}(r_s)$ is determined by the compressibility sum rule [1] using the compressibility according to the analytical expression available in the literature [19]. $C_{23c}(r_s)$ is fixed by the Shaw–Kimball relation [20] $G(q \to \infty) = 1 - g(0)$ using the sum-rule approach: $C_{23c}(r_s) = 0.846 r_s^{3/4}/[1 - g(0)]$ [9]. For $g(0)$ we use the analytical expression [21] $g(0) = [z/I_1(z)]^2/8$ with $z = 1.629 r_s^{1/2}$. $I_1(z)$ is the first-order modified Bessel function. $C_{33c}(r_s)$ is calculated using the relation between the pair-correlation function $g(0)$ and the static structure factor. For $r_s = 10$ we obtain $C_{13c} = 2.384$, $C_{23c} = 4.778$, and $C_{33c} = 3.554$. It can be shown [18] that the LFC $G_c(q)$ reproduces the results of recent Monte Carlo calculations [22].

We have studied $V_{sc,t}(r_M)$ and r_M versus r_s with the LFC as given in equation (19) and our results are shown in the inset of figure 1 as dashed–dotted lines. For $r_s < 10$ the screened potential is slightly less attractive while r_M is practically unmodified. The dashed–dotted line in figure 1 represents the screened potential $V_{sc,t}(r)$ for $r_s = 10$ calculated with $G_c(q)$.

Our results for the bound-state energies using the LFC in equation (19) against r_s are shown in figure 8. At $r_s = 20$ the binding energies are reduced by about 8% if compared with the results obtained with the two-sum-rule approach for the LFC (compare with figure 2). The critical density parameter where the binding energy of the ground

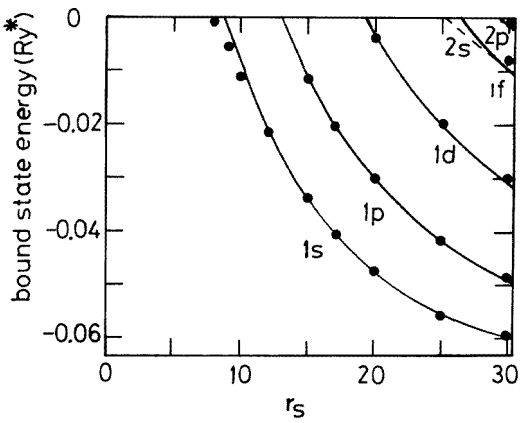

Figure 8. Bound-state energies E_{num} for a screened repulsive test charge found by matrix diagonalization against r_s as solid dots. The variational results E_{min} are shown as solid lines. The LFC according to equation (19) is used in the calculation.

state vanishes increases from $r_{sc} = 6$ to $r_{sc} = 8$. This is the result obtained by matrix diagonalization. With the variational method we find $r_{sc} = 9$ if we use $G_c(q)$ and $r_{sc} = 7$ for $G(q)$.

Together with our analysis of bound states in a screened repulsive potential using the RPA and the HA for the LFC (see table 1) we conclude that the detailed form of the LFC is important for a quantitative estimate of r_{sc} and the binding energy near r_{sc}. However, at lower density $r_s > 12$ the detailed form of the LFC is of minor importance if exchange and correlation effects are taken into account in the LFC within an approximative approach.

4. The screened attractive test charge

4.1. The attractive test-charge potential

Our two methods (the matrix diagonalization and the variational approach) can be easily applied for an attractive test charge. The effects of screening within the RPA [23, 24] and including the LFC [25] have already been considered in the literature. Nevertheless, we want to point out that in the literature the variational method for the ground state only has been applied and that the method of the matrix diagonalization is more general. Moreover we also discuss excited states. For the classification of the states we use the notation of the hydrogen atom with n and l.

The screened potential for an attractive test charge versus r is shown in figure 9 for $r_s = 5$. Note that already for $r_s = 5$ differences are seen between the screened potential according to the RPA and when the LFC is taken into account. Many-body effects via the LFC lead to a weaker attractive potential; therefore, the binding energy is reduced.

4.2. Matrix diagonalization

The numerical results for the 1s state versus r_s are shown in figure 10 within the RPA, the HA, and by using the LFC. Note that the finite LFC reduces the binding-state energy. The effect of the LFC is quite large for $2 < r_s < 6$, which is the density range of simple metals. With increasing density the binding energies decrease due to screening effects and vanish at a critical density, which is Mott's density N_M [10].

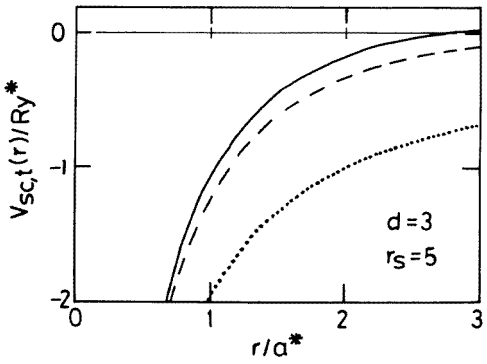

Figure 9. Screened Coulomb potential $V_{sc,t}(r)$ of an attractive test charge against distance r for $r_s = 5$ as the solid line. The dotted line represents the unscreened potential. The dashed line represents the RPA approximation.

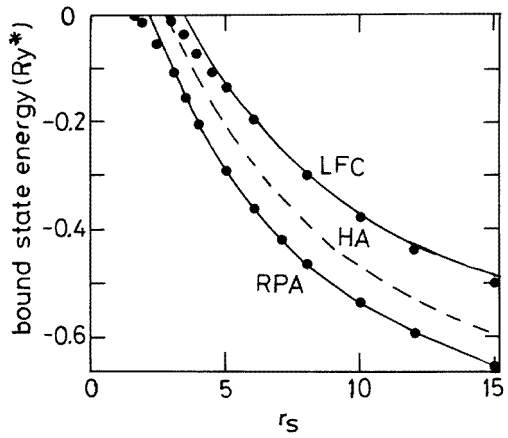

Figure 10. Ground-state energies E_{num} for a screened attractive test charge found by matrix diagonalization against r_s as solid dots. The variational results E_{min} (characterized by the variational parameter ν) are shown as solid lines. The HA is shown as the dashed line.

We mention that $N^{1/3}a^* = 0.62/r_s$ and, accordingly, N_M is related to a critical density parameter r_{sM}. For the ground state we obtained $r_{sM} = 1.7 (N_M^{1/3}a^* = 0.36)$ by using the RPA and $r_{sM} = 2.5$ $(N_M^{1/3}a^* = 0.25)$ by using the LFC.

4.3. The variational approach

In general we find excellent agreement of the matrix diagonalization with the variational energy obtained by using the variational method. For the ground state we use

$$\phi_{4\nu}(r) = A\,\mathrm{e}^{-r/2\nu}. \tag{20}$$

With this wave function for the 1s state we obtain

$$\langle T\rangle = \mathrm{Ryd}^* \frac{a^{*2}}{4\nu^2} \tag{21}$$

$$\langle V_l \rangle = \mathrm{Ryd}^* \frac{a^{*2}}{\nu^2} \frac{l(l+1)}{2} \tag{22}$$

and

$$\langle V_{sc,t} \rangle = \frac{1}{2\pi^2} \int_0^\infty \mathrm{d}q q^2 V_{sc,t}(q) \frac{1}{(1+q^2\nu^2)^2}. \tag{23}$$

Note that $\langle V_l \rangle = 0$ for $l = 0$ (1s state). Equation (23) is in agreement with the variational method used in [23]. Our results for the ground-state energy obtained with the variational method are shown in figure 10. Results within the HA are also shown. For $r_s > 1.5 r_{sM}$ a very good agreement is obtained between the two methods. For Mott's critical density we derive $r_{sM} = 2.12$ ($N_M^{1/3} a^* = 0.29$) within the RPA and $r_{sM} = 3.3$ ($N_M^{1/3} a^* = 0.19$) if the LFC is used.

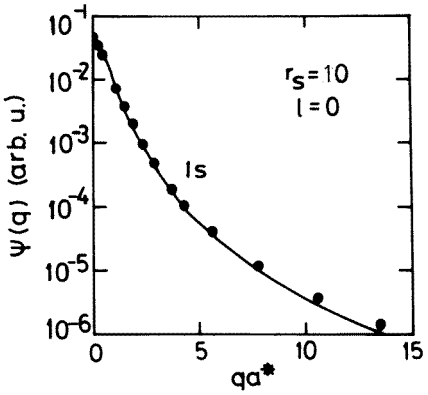

Figure 11. Wave function $\psi(q)$ of the 1s state for a screened attractive test charge for $r_s = 10$ against q when the LFC is taken into account. The solid dots represent the numerical results of the matrix diagonalization and the solid line represents the variational calculation according to equation (24) with $\nu = 0.513 a^*$.

The Fourier transform of $\phi_{4v}(r)$ is given by [17]

$$\phi_{4v}(q) \propto 1/(1+4q^2\nu^2)^2. \tag{24}$$

In figure 11 we show $\phi_{4v}(q)$ versus q for $r_s = 10$ with the LFC taken into account. The results obtained with the method of matrix diagonalization are also shown.

For the first excited state, which is the 2s state, we use

$$\phi_{5v}(r) = A(1 - rD)\,\mathrm{e}^{-r/2\kappa}. \tag{25}$$

The different energies for the variational energy are given by

$$\langle T \rangle = \mathrm{Ryd}^* \frac{a^{*2}}{4\kappa^2} \frac{(1 - 2\kappa D + 4\kappa^2 D^2)}{(1 - 6\kappa D + 12\kappa^2 D^2)} \tag{26}$$

and

$$\langle V_{sc,t} \rangle = \frac{1}{2\pi^2} \frac{1}{(1 - 6\kappa D + 12\kappa^2 D^2)} \int_0^\infty \mathrm{d}q q^2 V_{sc,t}(q) \left\{ \frac{1}{(1+q^2\kappa^2)^2} - 2\kappa D \frac{3 - q^2\kappa^2}{(1+q^2\kappa^2)^3} + 12\kappa^2 D^2 \frac{1 - q^2\kappa^2}{(1+q^2\kappa^2)^4} \right\} \tag{27}$$

with $\langle V_l \rangle = 0$ for $l = 0$. Note that $\langle \phi_{1s} | \phi_{2s} \rangle = \langle \phi_{4v} | \phi_{5v} \rangle = 0$, which implies that $D = (1/\nu + 1/\kappa)/6$.

For the second excited state, the 2p-state, we use

$$\phi_{6v}(r) = Ar\mathrm{e}^{-r/2\mu} \tag{28}$$

and we obtain

$$\langle T\rangle = \mathrm{Ryd}^* a^{*2}/4\mu^2 \tag{29}$$

$$\langle V_l\rangle = \mathrm{Ryd}^*(a^{*2}/\mu^2) l(l+1)/12 \tag{30}$$

and

$$\langle V_{sc,t}\rangle = \frac{1}{2\pi^2}\int^{\infty} \mathrm{d}q\, q^2 V_{sc,t}(q)\frac{1-q^2\mu^2}{(1+q^2\mu^2)^4} \tag{31}$$

with $\langle V_l\rangle = \mathrm{Ryd}^*\, a^{*2}/6\mu^2$ for $l = 1$. Our variational wave functions for an attractive test charge behave as $\phi_{6v}(r \to 0) \propto r^l$.

Table 2. Bound-state energies E_{min} for a screened attractive test charge for the states 1s ($\phi_{4v}(r)$), 2s ($\phi_{5v}(r)$), and 2p ($\phi_{6v}(r)$) found by the variational method using the LFC $G(q)$ together with the variational parameters for different r_s values

	(1s)		(2s)		(2p)	
r_s	ν/a^*	E_{min}/Ryd*	κ/a^*	E_{min}/Ryd*	μ/a^*	E_{min}/Ryd*
100	0.500	−0.8162	1.008	−0.0690	1.008	−0.0667
80	0.500	−0.7927	1.012	−0.0471	1.013	−0.0458
60	0.500	−0.7579	1.022	−0.0158	1.025	−0.0134
40	0.501	−0.6980	—		—	
20	0.503	−0.5619	—		—	
10	0.513	−0.3711	—		—	
5	0.558	−0.1339	—		—	
4	0.598	−0.0586	—		—	
3.5	0.644	−0.0126	—		—-	

Within the RPA and using the variational approach we did not find excited states for $r_s < 17.8$. The Mott density characterized by r_{sM} where the binding energy vanishes is $r_{sM} = 17.8$ for the 2s state and $r_{sM} = 19.8$ for the 2p state. Including the LFC we found excited states for $r_s > r_{sM} = 52$ for the 2s state and $r_s > r_{sM} = 54$ for the 2p state. The excited states have small binding energies (see table 2, where our variational results including the LFC are given). Using the RPA we have checked for the 2s state and the 2p state that for $r_s \to \infty$ we get -0.25 Ryd*, the binding energy of the unscreened hydrogen atom. More details on excited states will be published elsewhere.

5. Discussion

5.1. Application

For three dimensions the energy values for the bound states found for the screened *repulsive* test charge are much smaller than those found for quasi-one-dimensional [5] and two-dimensional [6] systems. This means that many-body effects for the screening function in three dimensions are less important than in low-dimensional systems. Our analysis of the wave function shows that for the ground state the (bound) electron density is greatly depleted around the charged centre in order to avoid the repulsive Coulomb potential at

small distances. The bound states are very extended in space due to the repulsive core for $r \to 0$, (see table 1, figure 3, and figure 5).

Let us assume that we place two negative test charges into a metal and the screening is provided by the electrons of the metal. Bound states should exist for $r_s > r_{sc} = 6$–8. Ordinary metals such as Na, Al, and Cu have larger density. However, the alkali metals K, Rb, and Cs have lower density, $r_s = 4.9$, 5.2, and 5.6, respectively. We conclude that K, Rb, and Cs are *not* very far away from the critical density where bound states can be expected. Many materials exist which are considered to be strongly correlated. We mention doped fullerenes, organic conductors, Chevrel phases, heavy fermions, and alloys. Cuprates are better described as a two-dimensional electron gas with $r_s > 4$.

For the metal-doped fulleride K_3C_{60} with a carrier density $N \approx 2 \times 10^{21}$ cm^{-2} (1 conduction electron per C_{60} which forms a sphere with a diameter of about 10 Å) we find $r_s \approx 9.3$ assuming for the effective Bohr radius $a^* = 0.53$ Å. This choice seems to be justified: experiments [26] indicate that an effective mass of $m^* \approx 5m_e$ and a background dielectric constant of $\varepsilon_L \approx 5$ are reasonable values. A Fermi energy of about $\varepsilon_F = 100$ meV is compatible with $r_s = 10$ and $a^* = 0.53$ Å. This estimate shows that strongly correlated molecular metals with $r_s \gtrsim r_{sc} \approx 6$–$8$ can be found in nature.

As far as we know no definitive conclusions have been derived concerning experimental results for the importance of many-body effects (exchange and correlation) for attractive impurities. However, we think that the predictions for attractive impurities are more easy to verify in experiment. We hope that a systematic study of positively charged impurities in ordinary metals with $1 < r_s < 5$ could give a definite answer. Doped semiconductors with $3 < r_s < 5$ are expected to be strongly disordered. The results of the present paper should be relevant for exciton physics in the metallic regime. Of course, the reduced mass should be used for the effective mass defining the effective Bohr radius and the effective Rydberg.

Let us recall that bound-state energies of screened attractive impurities are usually calculated within the variational approach [10, 23–25]. Our method using the matrix diagonalization is exact. New results for the case of an attractive test charge are the calculations of Mott's critical density for excited states and the bound-state energy of excited states. For the ground state our exact method gives a Mott density in good agreement with earlier results from the literature where a variational wave function of Hultyén type was used [24, 25]. The LFC leads to a reduction of the binding energy compared to the results in the RPA with $G(q) = 0$.

5.2. Theory and method

In [4] the effective electron–electron interaction potential for two-dimensional systems has been calculated (using the HA) within the Kukkonen and Overhauser approach [27]. In the present paper we discussed the screened potential and the test charge–test charge interaction: the calculated bound states are the bound states of two test charges screened by the electron gas.

Comparing our results [4] for the (screened) test charge–test charge interaction with the more profound Kukkonen and Overhauser approach for two-dimensional systems we conclude that our study of a screened potential gives already a good estimate of the importance of exchange and correlation for the effective electron–electron interaction, compare figure 1 in this paper with figure 4 in [4]. Therefore, we believe that our study of a repulsive test charge has important implications for superconductivity [11] and for the physics of the Wigner crystal [12] in strongly correlated electron systems. We would like to point out that we are working with a *realistic* interaction potential where the strength

is given by Coulomb's law. In this sense our theory is free of parameters. Let us finally note that a correct description of many-body effects via the LFC must be used in any theory which is intended to be applied to real materials with $r_s > 1$. In this density range electron–electron interaction effects are strongly modified by exchange and correlation.

One may ask whether the linear screening approximation used in this paper is valid. We expect that for *repulsive* test charges non-linear screening effects are smaller than for attractive test charges because (i) the wave functions are very extended compared to the effective Bohr radius (for the repulsive case the extension of the wave function is a factor of ten larger than for the attractive case, see figure 3) and (ii) the binding energies are small compared to the effective Rydberg. For *attractive* test charges non-linear screening effects are important: for a recent review concerning a proton in jellium see [28]. For instance, Mott's critical density is found as $r_{sM} = 2.06$ while we found $r_{sM} = 2.5$ using the matrix diagonalization with the LFC. It is clear that our values obtained for the binding energy can only be considered as a qualitative estimate because we used the linear screening approximation.

For the *attractive* case one might expect that at very low-density a test charge may form a D^- state (two electrons bound by a positively charged impurity). This problem requires the inclusion of two electrons in the Hamiltonian and cannot be discussed within the present one-electron approach.

6. Conclusion

In this paper we have studied bound states of negative and positive test charges located in the three-dimensional electron gas of given density. For an attractive test charge many-body effects included in the screening function reduce the binding energy of the ground state and of the excited states. A variational wave function with exponential long-distance behaviour is most appropriate for an attractive test charge.

At low electron density $r_s > r_{sc} \approx 6$–8 we find bound states for a repulsive test charge. The binding energy of the ground state saturates at low-density at about -0.065 Ryd*. Such states might be observed in strongly correlated metals and might be relevant for pairing (superconductivity) between equally charged carriers. For a repulsive test charge a variational wave function with Gaussian long distance behaviour is most appropriate.

Two methods have been developed to calculate the binding energies and the wave functions of the bound states in systems where the interaction potential in the momentum space is known in analytical form. In general we found for the ground state and the excited states very good agreement between the two methods. The variational approach is, from a practical point of view, the most important method because it can be applied very easily to more complex situations. Our result that bound states exist of a screened negative test charge using the RPA, the HA, and two different forms for the LFCs indicates that attraction can be expected in the three-dimensional electron gas. This prediction should be tested by experimenters. Our theoretical considerations for $r_s < 5$ should apply to normal metals while $r_s > 5$ is realized in molecular metals.

Acknowledgments

The Laboratoire de Physique des Solides (ERS 111) and the Groupe de Physique des Solides (URA 17) are laboratoires associés au Centre National de la Recherche Scientifique (CNRS).

References

[1] Pines D and Nozières P 1966 *The Theory of Quantum Liquids* vol 1 (New York: Benjamin)
[2] Mahan G D 1990 *Many-Particle Physics* (New York: Plenum) pp 449–55
[3] Friedel J 1953 *Adv. Phys.* **3** 446
[4] Gold A 1994 *Phil. Mag. Lett.* **70** 141
[5] Calmels L and Gold A 1995 *Phys. Rev.* B **51** 8426
[6] Ghazali A and Gold A 1995 *Phys. Rev.* B **52** 16 634
[7] Singwi K S, Tosi M P, Land R H and Sjölander A 1968 *Phys. Rev.* **176** 589
[8] Singwi K S and Tosi M P 1981 *Solid State Physics* vol 36 (New York: Academic) pp 177
[9] Gold A and Calmels L 1993 *Phys. Rev.* B **48** 11 622
[10] Mott N F 1949 *Proc. Phys. Soc.* **162** 416; 1982 *Proc. R. Soc. Lon.* A **382** 1
[11] Kohn W and Luttinger J M 1965 *Phys. Rev. Lett.* **15** 525
[12] Wigner E 1934 *Phys. Rev.* **46** 1002
[13] Moulopoulos K and Ashcroft N W 1993 *Phys. Rev.* B **48** 11 646
[14] Hubbard J 1957 *Proc. R. Soc.* A **243** 336
[15] Landau L and Lifchitz E 1966 *Mécanique Quantique* (Moscow: Mir)
[16] Flügge S 1974 *Practical Quantum Mechanics* (Berlin: Springer) problems 76–78
[17] Gradshteyn I S and Ryzhik I M 1980 *Table of Integrals, Series, and Products* (New York: Academic)
[18] Gold A 1996 unpublished
[19] Perdew J P and Yang Y 1992 *Phys. Rev.* B **45** 13 244
[20] Shaw R W Jr 1970 *J. Phys. C: Solid State Phys.* **3** 1140
Kimball J C 1973 *Phys. Rev.* A **7** 1648
[21] Yasuhara H 1972 *Solid State Commun.* **11** 1481
[22] Bowen C, Sugiyama G and Alder B J 1994 *Phys. Rev.* B **50** 14 838
Moroni S, Ceperley D M and Senatore G 1995 *Phys. Rev. Lett.* **75** 689
[23] Krieger J B and Nightingale M 1971 *Phys. Rev.* B **4** 1266
[24] Greene R L, Aldrich C and Bajaj K K 1977 *Phys. Rev.* B **15** 2217
Aldrich C 1977 *Phys. Rev.* B **16** 2723
[25] Borges A N O, Hipolito O and Campos V B 1995 *Phys. Rev.* B **52** 1724
[26] Palstra T T and Haddon R C 1994 *Solid State Commun.* **92** 71
[27] Kukkonen C A and Overhauser A W 1979 *Phys. Rev.* B **20** 550
[28] Hoffmann G G and Pratt R P 1994 *Mol. Phys.* **82** 245